International Journal of Multiphase Flow 57 (2013) 38–48

Contents lists available at SciVerse ScienceDirect

International Journal of Multiphase Flow

journal homepage: www.elsevier.com/locate/ijmulflow

Axial development of annular, churn and slug flows in a long vertical tube

Paulo J. Waltrich [a,*], Gioia Falcone [b], Jader R. Barbosa Jr. [c]

[a] Department of Petroleum Engineering, Louisiana State University, Baton Rouge, LA 70803, USA
[b] Institute of Petroleum Engineering, TU Clausthal Agricolastraße 10, 38678 Clausthal-Zellerfeld, Germany
[c] Polo – Research Laboratories for Emerging Technologies in Cooling and Thermophysics, Department of Mechanical Engineering, Federal University of Santa Catarina, Florianópolis, SC 88040900, Brazil

ARTICLE INFO

Article history:
Received 26 November 2012
Received in revised form 6 May 2013
Accepted 18 June 2013
Available online 16 July 2013

Keywords:
Annular flow
Churn flow
Slug flow
Axial development
Long tube
Vertical flow
Two-phase flow

ABSTRACT

Experimental data are presented on the axial development of gas–liquid flows in a 42-m long, 0.048-m ID tube system. Different transitional models for slug, churn and annular flow regimes were compared with visual observations and showed reasonable agreement for locations $L/D = 560$ and 820. The behavior of liquid holdup and frequency of flow structures (large waves, disturbance waves) were also analyzed for three different axial positions ($L/D = 102$, 521 and 815), over a range of pressure between 1.4 and 5.2 bar, liquid mass fluxes ranging from 17 to 319 kg m^2-s and dimensionless gas velocities from 0.05 to 1.6. The liquid holdup showed significant axial variation at all monitoring locations for higher liquid mass fluxes, while it appeared that a kind of developed flow was reached at $L/D = 521$ for lower liquid mass fluxes. The flow structure frequency did not exhibit significant axial variation for dimensionless gas velocities (Wallis parameter) between 0.2 and 1.6.

1. Introduction

The characterization of axial flow development leading to the transition between flow patterns has important practical applications, particularly for the types of multiphase flows encountered in the oil and gas industry where the length of pipelines are of the order of thousands of pipe diameters. State-of-the-art computer codes for the solution of multiphase flows in pipes rely on the identification of two-phase flow regimes (or flow patterns) for a proper selection of mechanistic models and closure relationships. Despite the large body of work available in the literature on flow regime prediction in vertical gas–liquid flows (Collier and Thome, 1996; Brennen, 2005; Ghiaasiaan, 2007), there is still a lack of studies addressing the axial development of flow regimes in pipes longer than 500 diameters or so.

Brown et al. (1975) and Wolf et al. (2001) investigated experimentally the flow development leading to hydrodynamic equilibrium in gas–liquid annular flow in heated and unheated vertical pipes. In addition to measurements of the axial change in pressure gradient and wall shear stress, they measured the evolution of the droplet entrained fraction (film flow rate), film thickness and interfacial wave characteristics (velocity and frequency). In both sets of experiments, the droplet entrainment fraction took longer distances to develop, as well as the film thickness in the unheated tube wall cases. Brown et al. (1975) noticed that the wave spectrum in a 9.61-mm ID tube took fairly long distances to develop, while according to Wolf et al. (2001) the parameters associated with the wave structure (disturbance wave velocity and frequency) showed only a small variation between z/D (i.e., distance/diameter) of 100 and 300 in a 31.8-mm ID tube for all mass flux combinations of air and water (10–120 kg/m^2-s for water and 71–154 kg/m^2-s for air). More recently, Hazuku et al. (2008) measured the evolution of the film thickness and wave characteristics in vertical annular flow in a 3-m long, 11-mm ID pipe by means of a laser focus displacement technique. It was concluded that the flow did not reach a developed state in the test section because neither the film thickness nor the wave frequency ceased to decrease as a function of distance.

Van Hout et al. (2001) studied the evolution of slug flow in two 10-m long vertical pipes – one with an internal diameter of 0.024 mm ($L/D = 416.7$) and another of 0.054 mm ($L/D = 185.2$) – for liquid superficial velocities of 0.01, 0.1 and 0.25 m/s and gas superficial velocities of 0.41 and 0.63 m/s. Both the Taylor bubble and the liquid slug lengths were seen to increase with distance in the two systems, and some evidence of coalescence in the larger pipe was observed near the top end of the larger pipe.

* Corresponding author.
E-mail address: waltrich@lsu.edu (P.J. Waltrich).

0301-9322/$ - see front matter © 2013 Elsevier Ltd. All rights reserved.
http://dx.doi.org/10.1016/j.ijmultiphaseflow.2013.06.008

Kaji et al. (2009) investigated the effect of the flow development length on the structure of slug flow in vertical pipes. In addition to void fraction, the lengths and frequencies of Taylor bubbles and liquid slugs were reported at several distances from the inlet for a 51.2-mm ID, 3.5-m long (L/D = 68.4) and for a 52.3-mm ID, 9-m long (L/D = 172) test section. The Taylor bubble and the liquid slug lengths also increased with distance, reaching somewhat stable values at z/D = 100. The slug frequency, however, showed a gradual decrease which did not stabilize until the end of the test section. A correlation for the gas superficial velocity-based Strouhal number as a function of the Martinelli parameter was proposed.

As far as churn flow is concerned, although some researchers confirmed its existence as a separate flow regime (Hewitt and Jayanti, 1993; Jayanti et al., 1993; Azzopardi and Wren, 2004), some confusion has been generated in the past due to the association of the term "churn flow" with a type of developing slug flow (Mao and Dukler, 1993). Barbosa et al. (2001), Da Riva and Del Col (2009) and Wang et al. (2012) investigated the flow development and wave behavior in churn flow. However, their analyses were limited to the region near the entrance. One of the few studies about axial development of vertical flow regimes which included churn flow was conducted by Julia et al. (2009), who investigated the axial development of flow regimes in vertical upward flow in an annulus. The inner and outer diameters of the annulus for their study were 19.1 and 38.1 mm, respectively, and a total vertical length of 4.37 m. Their flow conditions included a range of superficial gas velocities between 0.01 and 30 m/s, and superficial liquid velocities between 0.2 and 3.5 m/s. However, only a few runs were carried out for churn/annular flows, since these flow regimes were not the focus of their work.

From the studies regarding axial flow development, there emerges a clear need for more experimental data on the evolution of gas–liquid flows in vertical pipes longer than 500 diameters. Therefore, a particular aim of this work is to evaluate experimentally the axial development of gas–liquid flows in a long vertical tube (42-m long, 0.048-m ID, L/D = 875) at conditions where annular, churn and slug flows are observed. The results provide confirmatory quantitative evidence of the existence of both slug and churn flow regimes as independent two-phase flow patterns in a very long tube.

Additionally, data are presented on the behavior of the liquid holdup as a function of distance in a very long tube for conditions at which the slug and churn flow regimes are expected to occur according to well-established models available in the literature (Brauner and Barnea, 1986; Jayanti and Hewitt, 1992). The prediction of the transition to churn flow according to the models of Brauner and Barnea (1986) and Jayanti and Hewitt (1992), which were developed based on data for shorter flow loops (L/D < 300), is assessed in a longer tube for pressures up to 5 bar. Moreover, data on the frequency of periodic flow structures in churn flow (large waves and disturbance waves) derived from the experimental measurement of liquid holdup at different positions along the test section are used to analyze the flow development of churn flow in a long vertical tube.

2. Experimental facility and procedure

A large-scale air–water experimental two-phase flow loop was constructed at Texas A&M University (the TowerLAB facility), whose test section consists of a series of 0.048-m ID transparent PVC pipe segments, comprising a total tube length of 42 m (875 diameters), as shown in Fig. 1.

A centrifugal pump (Dayton 2PC38) is used to pump water from a 662-L water tank to the test section. The water flow rate is controlled using a variable speed driver and an electronically-actuated valve downstream to the water pump. The water mass flow rate is measured using a Coriolis mass flow meter (Micro Motion F100). A water filter with a 10-μm pore size element is also connected just upstream to the mixing tee to keep the water free of particles and impurities. The uncertainty average for the water flow rate measurement was estimated as ±2 kg/h.

Compressed air is provided using a screw compressor (Ingersoll Rand 75H-SP), and measured using a vortex meter (Rosemount 8800D) and a Coriolis meter (Elite Micro Motion CMF050). The combination of two actuated valves in the air line (see Fig. 1) with a control valve (0.0508 m ball actuated valve) at the outlet of the test section provides a combined control of the pressure and gas flow rate. Air and water are mixed in a mixing tee, which consists of a 0.0508 m perforated nipple inserted in a 0.0762 m tee. The uncertainty average for the air flow rate measurement was estimated as ±2.5 kg/h.

In addition to direct visual observation of the flow configuration by means of high-speed and CCD (Charge-Couple Device) cameras, the experimental apparatus enables measurement of pressure gradient, liquid holdup (via conductivity probes) and slug/wave frequency over a range of pressures and phase flow rates. An overview of the distribution of the flow monitoring instrumentation along the test section is shown in Fig. 1.

For this study, absolute pressure measurements were performed at 5 different distances from the mixing tee: 18D, 207D, 437D, 689D, and 835D. Rosemount pressure transducers (DP3051) were used for the pressure measurements. Static pressure measurements were carried out using strain-gauge transducers connected to the test section via 6.25 mm ID nylon tubing filled with liquid (water) to avoid pressure signal damping due to bubble trapping. After calibration, the pressure measurement uncertainty average was estimated as ±0.3 kPa. Temperature signals were taken using T-type thermocouple probes, inserted inside the nylon pressure line taps.

The liquid holdup was measured using two-wire conductivity probes similar to those utilized by Zabaras et al. (1986), which consist of two parallel wires mounted perpendicularly to the flow direction (see Fig. 2). The probes were located at distances of 102D, 521D and 815D from the mixing tee. The electrical conductance between the wires is proportional to the amount of liquid between them. The cross-sectional liquid holdup is calculated from the measured local film thickness assuming symmetry with respect to the pipe centerline. To ensure a good linearity between the excitation and output signal, an electronic circuit was design and fabricated to generate an excitation signal, demodulate and amplify the output signal. The excitation signal consists of a square wave with a frequency of 100 kHz. The calibration procedure used here was also based on the work of Zabaras et al. (1986). However, their technique was adapted to provide better accuracy. The adapted calibration procedure consists of producing different levels of liquid height in a closed tube section with the two-wire sensor installed. Since the sensor can only capture the liquid level between the two wires, the calibration should not be significantly affected by the tube orientation (inclination). Therefore, the test section tube is set nearly horizontally, with one of its ends fitted with a transparent window. Thus, the different levels of liquid heights are captured by a digital camera placed in front of the transparent window. The digital pictures are stored in a computer and an image processing software (Photron, 2006) is used to measure the liquid levels. The measuring concept using this software consists of having a reference length scale present in the image, which can be used to calibrate the pixels size. After the size of the pixels is calibrated, the software provides the distance in the picture between any two points indicated by the user. The reference length scale in the present case is the diameter of the wires, which is previously measured using a micrometer. The liquid level

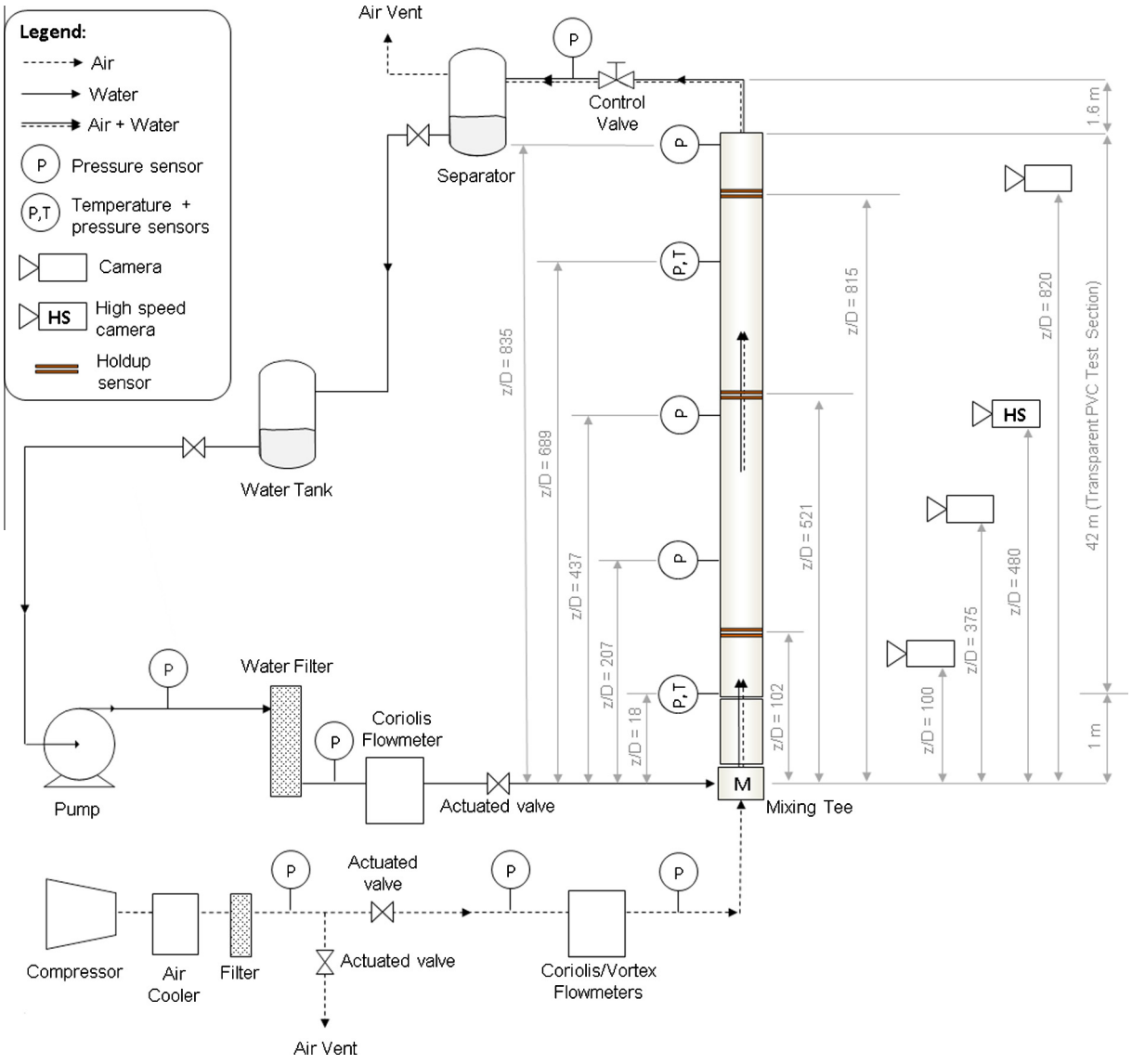

Fig. 1. Schematic view of the experimental two-phase flow loop.

is then obtained indicating in the picture the distance between the bottom of the wire and the liquid level surface. The liquid holdup measurement uncertainty average was estimated as ±0.02.

The measurements of pressure, temperature and liquid holdup were carried out via a data acquisition system at a sampling rate of 100 Hz. The data were recorded for a total time of 120 s, after steady state was reached. The total number of data points in a string was 12,000. The steady-state condition was considered to be established when the deviations of all measured quantities with respect to their mean values were lower than their experimental uncertainty.

The two-phase flow behavior was visually recorded using three CCD cameras and one high-speed camera, which were positioned as presented in Fig. 2. This visualization set up allowed synchronized video recording of the two-phase flow at four different locations (see Fig. 3). The videos recorded by the high-speed camera were captured at a rate of 250 frames per second for all tests performed in this work. Visual observations were made at locations $z/D = 100$, 480 and 820. The frequency of flow structures (large waves, disturbance waves) derived from the liquid holdup measurements were obtained at the three axial positions $z/D = 102$, 521 and 815. The experimental data were obtained over a range of absolute outlet pressures between 1 and 5.2 bar, liquid mass fluxes ranging from 15 to 315 kg/m^2-s and dimensionless superficial gas velocities – defined according to Wallis (1969) and presented in detail later – from 0.05 to 1.5.

3. Results and discussion

A table with the complete dataset of liquid and gas mass fluxes, superficial phase velocities, gas density, pressure and liquid holdup is included in the electronic annex linked to this paper. The information in this annex can be used to better understand some of the analyses performed in this work. Fig. 4 presents the percentage change in gas density between the inlet and outlet of the test section ($=(\rho_{G,in} - \rho_{G,out})/\rho_{G,in} \times 100$) for each test, based on the data provided in the electronic annex table.

Fig. 5 presents the Probability Density Functions (PDF) of the liquid holdup for three axial positions for gas and liquid mass fluxes of 4 and 110 kg/m^2-s, at an outlet pressure of approximately 2 bar. The gas and liquid superficial velocities at $z/D = 815$ are 1.68 and 0.11 m/s, respectively. The PDF of the liquid holdup was constructed dividing the 0–1 holdup domain into 250 equal-size bins of magnitude 0.004. Each holdup value of the acquired data string

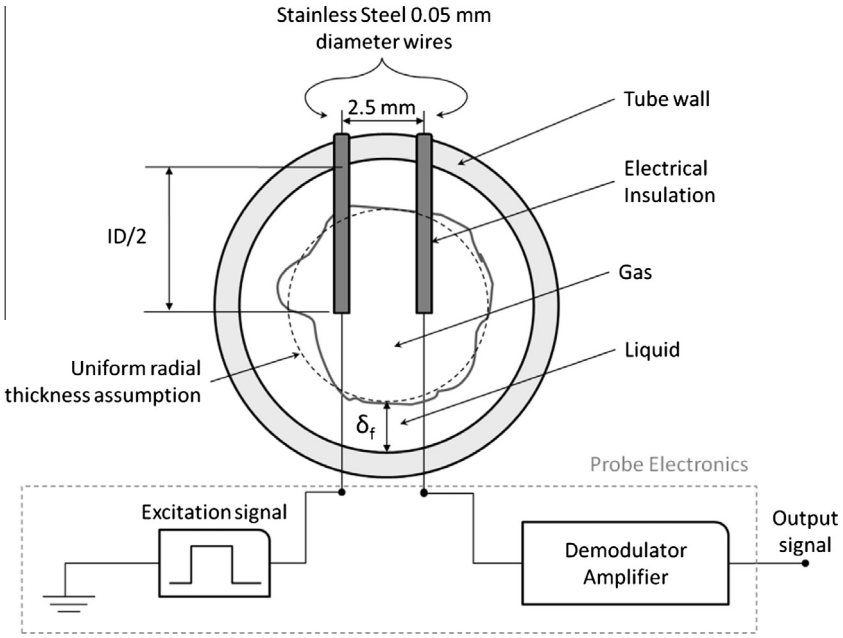

Fig. 2. Two-wire probe design used to measure liquid holdup.

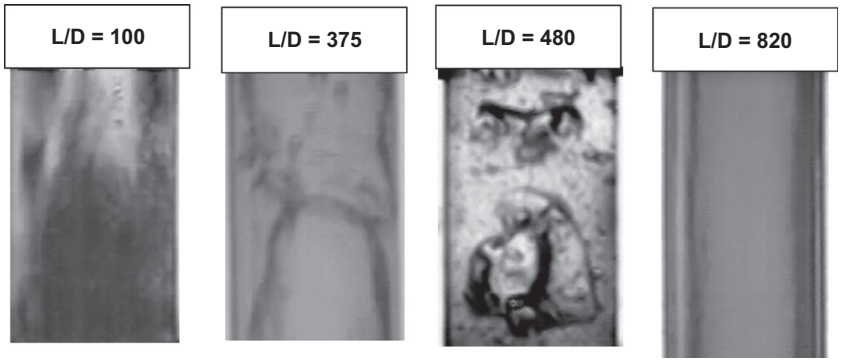

Fig. 3. Snapshots of the synchronized videos captured during an experimental run (M_G = 4 kg m^{-2} s^{-1}, M_L = 110 kg m^{-2} s^{-1} and at 2 bar pressure). The synchronized videos are used to recognize the flow regime and analyze the axial development of the flow.

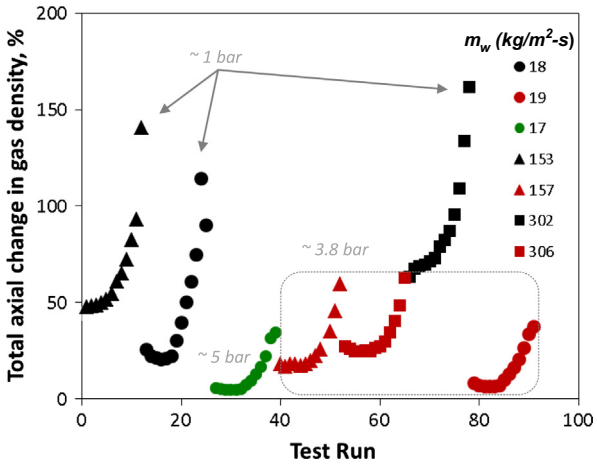

Fig. 4. Percentage of total axial change in gas density for the experimental runs.

that corresponded to the holdup interval of a particular bin was counted as one in that bin. The number of observations in each bin was normalized by the total number of data points in the acquired data string.

Liquid holdup measurements and their corresponding PDF distributions have been used to identify different flow regimes in two-phase flows, in similar manner to Lee et al. (2008), Mi et al. (1998) and Costigan (1997). As can be seen from Fig. 5, the PDF results for $z/D = 521$ and 815 show two distinct peaks at high and low liquid holdup levels, which agrees well with the expected structure of developed slug flow (high liquid holdup in the liquid slug and low liquid holdup in the Taylor bubble). On the other hand, the absence of two clear PDF peaks at $z/D = 102$ leads to the conclusion that the slug flow is still underdeveloped near the inlet. In fact, the correlation for the length of the slug flow entrance region $(z/D)_e$ of Dukler and Taitel (1986) given by:

$$(z/D)_e = 42.6\left[\frac{U_M}{(gD)^{0.5}} + 0.29\right] \quad (1)$$

provides, for the condition of Fig. 5, a value of $(z/D)_e = 83$, which corroborates the observed behavior. In Eq. (1), g is the acceleration due to gravity, D is the pipe diameter and U_M is the mixture superficial velocity, i.e., the sum of the phase superficial velocities.

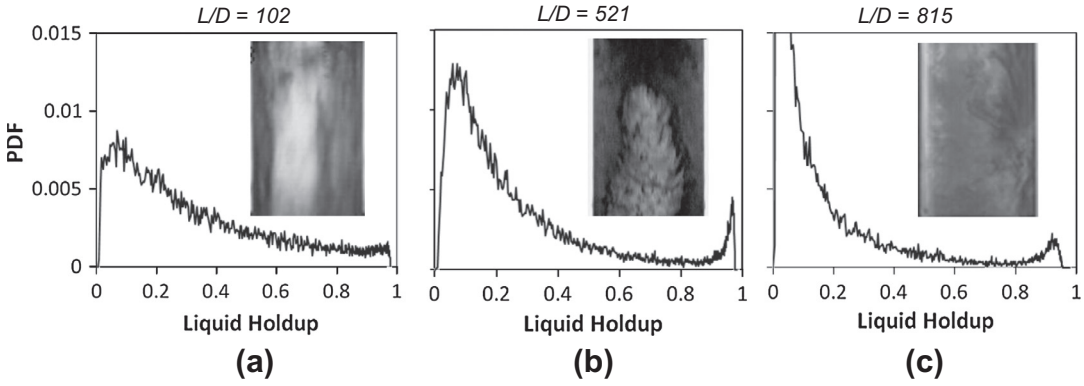

Fig. 5. Probability Density Function (PDF) of liquid holdup measurements at three different positions conditions leading to developed slug flow ($m'_G = 4$ kg m^{-2} s^{-1}, $m'_L = 110$ kg m^{-2} s^{-1} and at 2 bar outlet pressure).

Fig. 6 shows the holdup PDF results for gas and liquid mass fluxes of 16 and 155 kg/m^2-s, at an outlet pressure of approximately 3.8 bar. At this condition, the gas and liquid superficial velocities at $z/D = 815$ are 3.48 and 0.15 m/s, respectively. Only one PDF peak appears at this condition, which becomes more pronounced as z/D increases and the gas expands. Visual observation of the two-phase flow indicated that the flow pattern for this condition was churn flow, as can be seen in Fig. 6b. It is worth pointing out the similarity between the liquid holdup PDFs of underdeveloped slug flow and churn flow (especially at $z/D = 102$). For a short test section, this lack of a distinguishable feature between underdeveloped slug and churn flows may cause some confusion, as indeed it seems to have been the case with previous works in the literature (Mao and Dukler, 1993).

Another point that suggests the absence of underdeveloped slug flow at the test conditions of Fig. 6 is the consideration of the criterion based on the maximum void fraction developed by Brauner and Barnea (1986). These authors suggested that the collapse of the bubbles in the liquid slug in slug flows can be associated with a maximum value for the void fraction. Thus, based on a maximum bubble packing in the liquid slug, the transition from slug to churn flow should occur when the void fraction in the liquid slug reaches $h_{G,max} = 0.52$ (or minimum liquid holdup of $h_{L,min} = 0.48$).

From the PDFs for the liquid holdup shown in Fig. 6, it is possible to see that there are almost no measurements of liquid holdup greater than 0.48 for the axial location $z/D = 815$. In other words, the majority of the *likely* liquid slugs have collapsed at this point, while churn flow was observed for this axial location.

For locations $z/D = 102$ and 521, there is a greater number of times when the liquid holdup is higher than 0.48 for the measurements in Fig. 6, compared to location $z/D = 815$. Therefore, there is a higher probability for the presence of liquid slugs at these first two locations than for location $z/D = 815$. The correlation of Dukler and Taitel (1986) for the length of the entrance region in slug flow gives $(z/D)_e = 204$. Hence, the presence of a larger number of liquid holdup measurements greater than $h_{L,min} = 0.48$ also reinforces the idea of a flow regime developing region as observed by Dukler and Taitel (1986).

Fig. 7 presents a comparison between experimental data and models that were developed for predicting the slug-to-churn and churn-to-annular transitions for an outlet pressure of 1.4 bar. The data are presented as a function of the liquid and gas superficial velocities. The local superficial gas velocities were determined based on the inlet gas flow rate (kept fixed) and the local pressure at $z/D = 437$. Visual observations of the flow configuration using the high-speed camera were performed for each experimental run. Additionally, liquid holdup PDFs were used to render the characterization of flow regimes less subjective. As can be seen from Fig. 7, the occurrence of slug flow at positions far from the liquid inlet ($z/D = 480$) is in reasonable agreement with the transition models of Brauner and Barnea (1986) and Jayanti and Hewitt (1992) for lower pressures (1.4 bar) and lower superficial liquid velocities (<0.3 m/s). However, these models do not show a good match with the data at higher pressure (3.8 bar), as presented in Fig. 8. On the other hand, the slug to churn flow regime transition line of the Hewitt and Roberts (1969) map (obtained from numerical interpolation in terms of the phase momentum fluxes) shows a better match at higher pressures and superficial liquid velocities.

According to Brauner and Barnea (1986), the transition from slug flow to churn flow occurs when the liquid holdup in the liquid

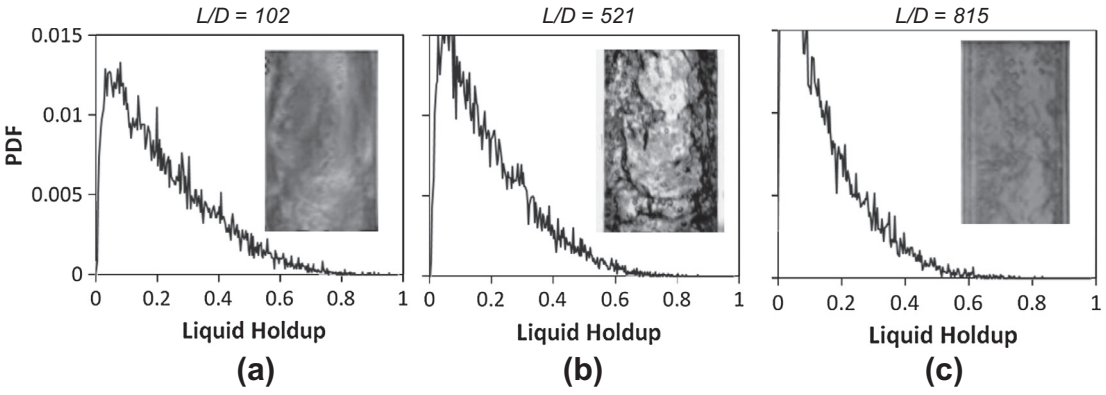

Fig. 6. Probability Density Function (PDF) of liquid holdup measurements at three different axial positions for conditions leading to developed churn flow ($m'_G = 16$ kg m^{-2} s^{-1}, $m'_L = 155$ kg m^{-2} s^{-1} and at 3.8 bar outlet pressure).

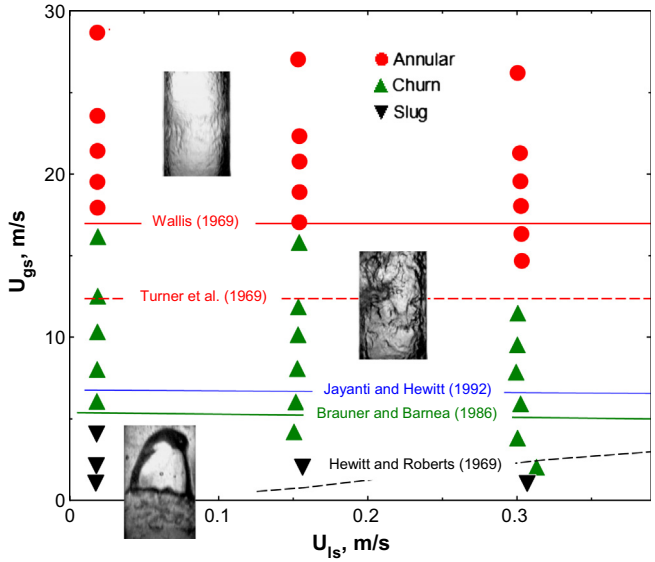

Fig. 7. Comparison between flow regime transition models and experimental observations at 1.4 bar and location $z/D = 480$.

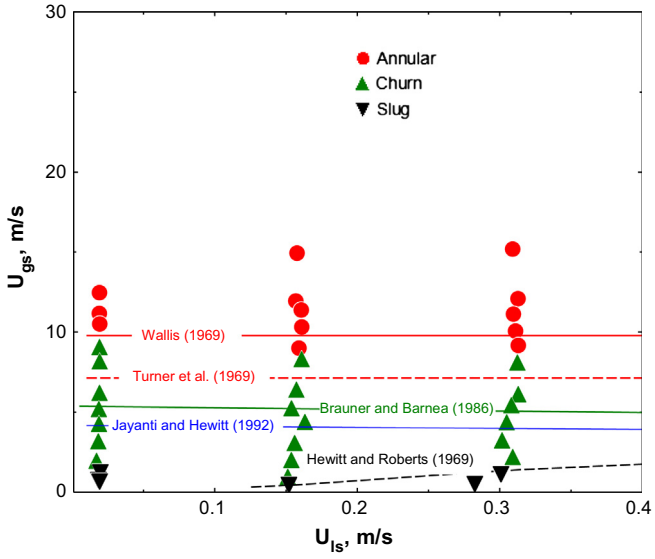

Fig. 8. Comparison between flow regime transition models and experimental observations at 3.8 bar and location $z/D = 480$.

slug falls below a minimum value of 0.48. The liquid holdup in the liquid slug for vertical flow, h_{sl}, is correlated by:

$$h_{sl} = 1 - 0.058\left\{2\left[\frac{0.4\sigma}{g(\rho_L-\rho_G)}\right]^{0.5}\left(\frac{2f_M U_M^3}{D}\right)^{0.4}\left(\frac{\rho_L}{\sigma}\right)^{0.6} - 0.725\right\}^2 \tag{2}$$

where ρ is the mass density and the subscripts G and L denote gas and liquid, respectively. f_M is the friction factor given by:

$$f_M = 0.046\left(\frac{v_L}{U_M d_T}\right)^{0.2} \tag{3}$$

where v is the kinematic viscosity.

The model of Jayanti and Hewitt (1992) assumes that the slug-churn transition is triggered by flooding in the Taylor bubble as the gas superficial velocity reaches a critical value. The following flooding-type correlation was proposed to identify the flow regime transition:

$$(U_{bS}^*)^{0.5} + m(U_{fS}^*)^{0.5} > 1 \tag{4}$$

where U_{bS}^* and U_{fS}^* are the dimensionless superficial Taylor bubble and liquid film velocities, respectively, and m is a factor that takes into account the length of the Taylor bubble on the transition velocity. The variables are defined as follows:

$$U_{bS}^* = U_{bS}\left[\frac{\rho_G}{gD(\rho_L-\rho_G)}\right]^{0.5} \tag{5}$$

$$U_{fS}^* = U_{fS}\left[\frac{\rho_L}{gD(\rho_L-\rho_G)}\right]^{0.5} \tag{6}$$

where

$$U_{bS} = \left(1-\frac{4\delta}{D}\right)\left\{1.2U_M + 0.35\left[\frac{gD(\rho_L-\rho_G)}{\rho_L}\right]^{0.5}\right\} \tag{7}$$

$$U_{fS} = U_{bS} - U_M \tag{8}$$

$$m = \begin{cases} 1; & \text{se } \frac{L_{TB}}{D} > 120 \\ 0.1928 + 0.01089\frac{L_{TB}}{D} - 3.754\times10^{-5}\left(\frac{L_{TB}}{D}\right)^2; & \text{se } \frac{L_{TB}}{D} \leqslant 120 \end{cases} \tag{9}$$

L_{TB} is the length of the Taylor bubble calculated from a mass balance in the liquid phase:

$$U_{LS} = U_{sl}h_{sl}\frac{L_{sl}}{L_{sl}+L_{TB}} - U_{fS}\frac{L_{sl}}{L_{sl}+L_{TB}} \tag{10}$$

where U_{LS} is the superficial liquid velocity, U_{sl} is the liquid slug velocity, L_{sl} is the liquid slug length and h_{sl} is the liquid holdup in the liquid slug. Jayanti and Hewitt (1992) suggested that, close to the flow regime transition, $U_{sl} = U_M$, $L_{sl} = 12D$ and $h_{sl} = 0.5$. An additional equation is necessary to relate the Taylor bubble falling film thickness, δ, and U_{fS}. Jayanti and Hewitt made use of the Brotz correlation given by:

$$U_{fS} = 39.66\frac{\delta}{D}\left\{gD\frac{(\rho_L-\rho_G)}{\rho_L}\left[1-\left(1-\frac{4\delta}{D}\right)^{0.5}\right]\right\}^{0.5} \tag{11}$$

Two relationships are often associated with the churn-annular flow transition, namely, the Wallis (1969) and the Turner et al. (1969) flow reversal criteria. According to Wallis (1969), the flow reversal transition is relatively insensitive to the liquid superficial velocity, and can occur at an approximately constant gas superficial velocity. For tubes smaller than 0.05 m in diameter, the flow reversal transition is correlated with the dimensionless superficial gas velocity as follows (Hewitt, 2010):

$$U_{GS}^* = U_{GS}\left[\frac{\rho_G}{gD(\rho_L-\rho_G)}\right]^{0.5} \approx 1 \tag{12}$$

For larger diameter tubes, droplet entrainment from the wave tips may occur before the waves themselves are transported (Hewitt, 2010). In this case, an alternative correlation for the flooding velocity that does not take into account the tube diameter has been suggested. This has been attributed to Pushkina and Sorokin (1969) and is written in terms of the Kutateladze number, Ku_G, as follows:

$$Ku_G = U_{GS}\left[\frac{\rho_G^2}{g\sigma(\rho_L-\rho_G)}\right]^{0.25} \approx 3.2 \tag{13}$$

where σ is the gas–liquid interfacial tension.

The above equation is similar to the Turner criterion for calculating the critical velocity for liquid loading in vertical and near vertical wells; the corresponding value of Ku_G in Turner's model is 3.08. In order to achieve this critical value of 3.08 for the Kutateladze number, one has to follow the Turner et al. (1969) assumption that the droplet Reynolds number ranges from 10^4 to 2×10^5 and the spherical droplet drag coefficient of spherical droplets in this range corresponds to approximately 0.44. The droplet diameter was estimated assigning a value of 30 for the droplet Weber number. As can be seen from Figs. 7 and 8, the Wallis (1969) criterion shows a good match with the experimental results. The Turner et al. (1969) criterion also shows a good agreement for the annular-to-churn flow transition, but only for high superficial liquid velocities. Comparisons between models and data similar to those presented in Figs. 7 and 8 were also carried out for the camera located at $z/D = 820$ (using the gas density derived from the pressure measurement at $z/D = 835$). The results were virtually the same as those presented above.

Fig. 9 presents the total pressure gradient as a function of distance, gas mass flux and pressure. Since only absolute pressure measurements were available along the test section, the total pressure gradient was calculated using two consecutive pressure measurements. For example, the pressure gradient indicated in Fig. 9 at $z/D = 689$ was calculated subtracting the pressure measurements between positions $z/D = 437$ and 689, and dividing by the distance between these two points. As can be seen from the data, there is no significant change in the pressure gradient along the test section for $U^*_{GS} > 0.3$, except for the condition in Fig. 9c for U^*_{GS} and $z/D > 437$. An explanation for the deviation in this case can be attributed to the flow restriction caused by the control valve (see Fig. 1), which decelerates the flow and reduces the pressure gradient near the outlet of the tube. For $U^*_{GS} < 0.3$, the results show a considerable variation of the pressure gradient with respect to distance. This variation is related to the combined effect of the gas expansion and axial flow development along the tube.

Fig. 10 presents the experimental results of time-averaged liquid holdup as a function of the dimensionless superficial gas velocity, U^*_{GS}, for different axial positions and for pressures between 1.4 and 3.8 bar. As can be seen, the liquid holdup decreases exponentially with $U^*_{GS}$and increases with the liquid mass flux, as shown in Fig. 10a and b. Fig. 10c and d also show that, for U^*_{GS} higher than 0.6, there is only a small difference in liquid holdup between the dimensionless axial positions $z/D = 102$, 521 and 815 for low pressure and liquid mass flux. In Fig. 10c, there is almost no difference in holdup between the distinct axial locations because of the low values of liquid holdup, which lie below the estimated measurement uncertainty (±0.02). Fig. 10d shows that for higher pressure and liquid mass flux there is a more significant axial change in liquid holdup.

The variation of the time-averaged liquid holdup with dimensionless axial position (z/D) is presented in Fig. 11. The liquid holdup varies more significantly between all axial positions for the liquid mass flux of 310 kg/m^2-s, while for 19 kg/m^2-s it seems to reach some sort of developed flow for all conditions presented,

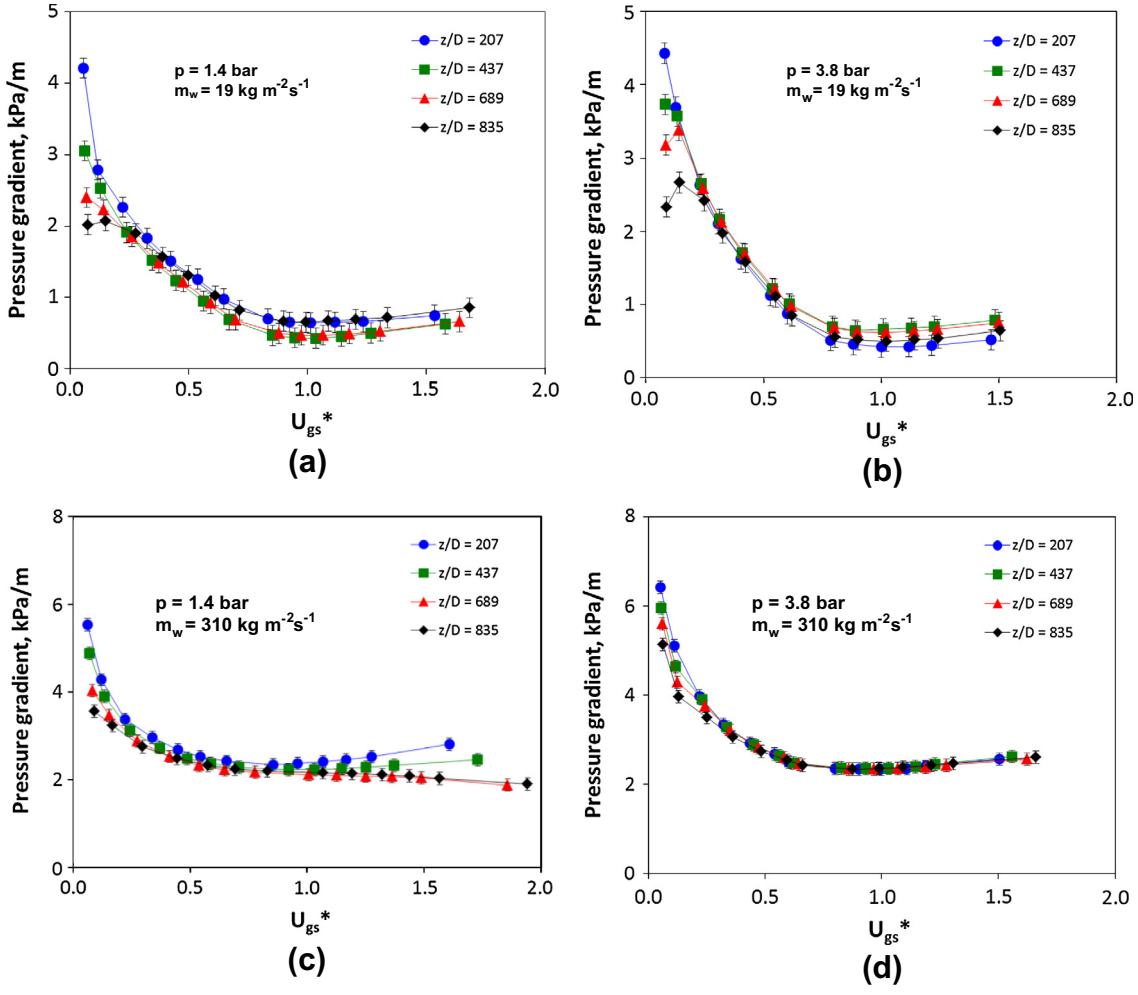

Fig. 9. Total pressure gradient as function of U^*_{GS} for different axial positions, liquid mass fluxes and pressure between 1.4 and 3.8 bar.

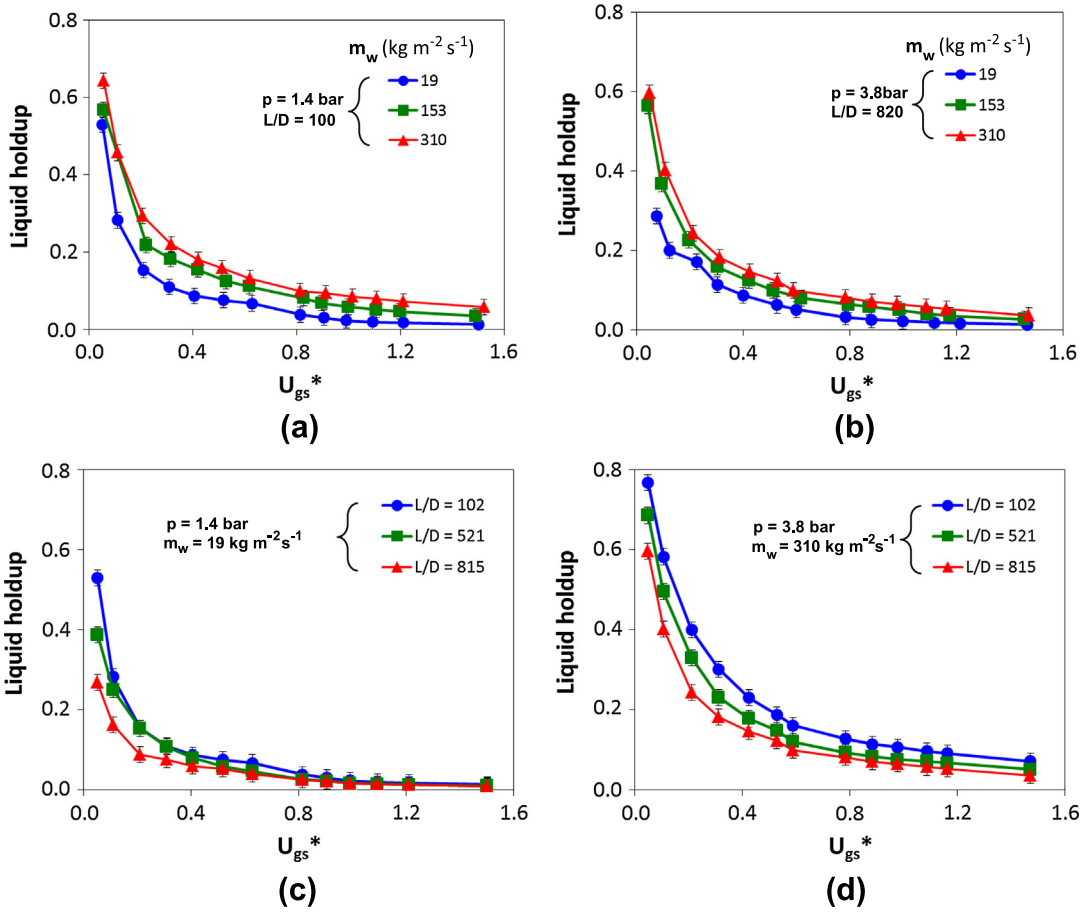

Fig. 10. Liquid holdup as function of U^*_{GS} for different axial positions, liquid mass fluxes and outlet pressures of 1.4 and 3.8 bar.

except for U^*_{GS} = 0.3. At a fixed liquid mass flux, the axial change in liquid holdup is due to a combined influence of gas expansion (due to pressure drop) and phase redistribution (axial flow development). It seems that, at high gas velocities (churn and annular flows), the holdup variation with distance is more affected by flow development than by gas expansion. For instance, the maximum axial variation observed in U^*_{GS} among all tests was 40%, while the liquid holdup between the positions z/D = 521 and 815 have changed as much as 200% (see Fig. 11a) for a liquid mass flux of 310 kg/m^2-s. Therefore, it is suggested that the flow has not reached a fully developed condition for a liquid mass flux of 310 kg/m^2-s in any of the cases reported in Fig. 11.

Fig. 12 shows the variation of the time-averaged normalized liquid holdup with U^*_{GS} for the axial position z/D = 521 at 1.4 bar pressure. The normalized liquid holdup is defined as the ratio of the values of liquid holdup at z/D = 521 and at z/D = 815 for specified values of U^*_{GS} and liquid mass flux. As can be seen, for liquid mass fluxes of 19 and 153 kg/m^2-s, it appears that the flow has attained a type of developed condition at z/D = 521, since the normalized liquid holdup at this position have values close to unity for the entire U^*_{GS} range. However, for U^*_{GS} > 1.0 and a liquid mass flux of 310 kg/m^2-s, the fully developed flow region does not seem to be reached, since the normalized liquid holdup diverges from unity. Fig. 13 shows the effect of the system pressure on the normalized liquid holdup, which deviates more markedly from unity at lower pressures.

Fig. 14 presents the frequency of flow structures (i.e., disturbance waves, churn flow waves) as a function of U^*_{GS} for three different axial positions, liquid mass fluxes varying from 19 to 310 kg/m^2-s, and pressures ranging from 1.4 to 5.2 bar. The flow structure frequency was calculated here using an approach similar to the one developed by Hazuku et al. (2008), who developed a technique to compute the number of large liquid flow structures in vertical annular flow. Since their technique is basically a method to identify and count portions of the holdup signal associated with high contents of liquid, it has been sought in the present work that this method could be extended to identify the occurrence of liquid flow structures in churn and slug flow. As suggested by Hazuku et al. (2008), a flow structure is here defined as a portion of the signal whose equivalent thickness peak is higher than that of the upper layer of the flow structure, and both ends are lower than the average film thickness. Fig. 15 shows a pictorial representation of flow structures in annular, churn and slug flow conditions. The upper structure layer is defined as (Hazuku et al., 2008):

$$\bar{\delta}_u = \frac{1}{n}\sum_{k=1}^{n}\delta_k, \quad (\delta_k > \bar{\delta}) \tag{14}$$

where $\bar{\delta}_u$ is the average upper structure layer thickness, δ_k is the instantaneous (equivalent) film thickness and $\bar{\delta}$ is the average (equivalent) film thickness. Since film thickness measurements can be related to the shape of the gas–liquid interface, the procedure developed by Hazuku et al. (2008) is expected to provide a reasonable representation of larger structures passing along the film thickness sensors. The structure frequency results are of the same order of magnitude as the wave frequency values reported by Hewitt et al. (1985) and Barbosa et al. (2001), i.e., between 5 and 22 Hz. However, the latter works did not take into account the axial flow development in their wave frequency analysis, as only waves formed near the inlet were evaluated. As can be seen from Fig. 14,

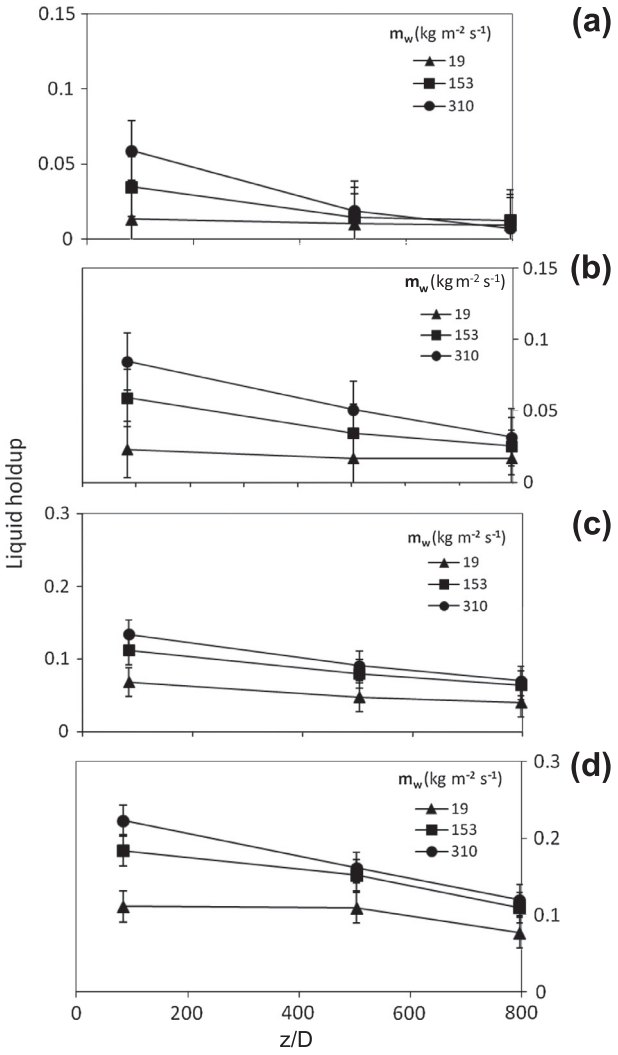

Fig. 11. Liquid holdup as function of axial position for of (a) 1.5, (b) 1.0, (c) 0.6 and (d) 0.3, at 1.4 bar pressure.

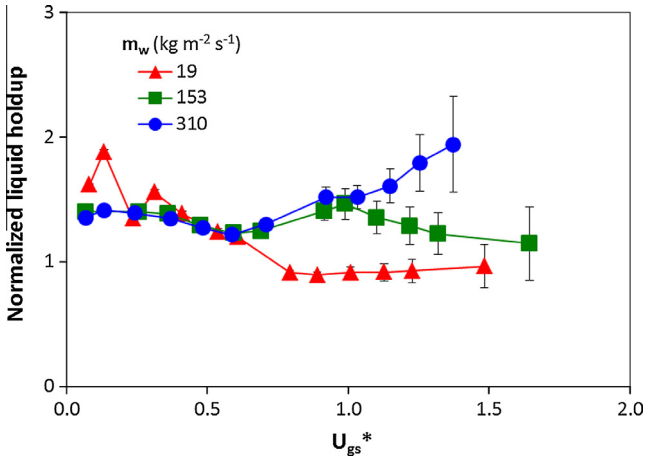

Fig. 12. Normalized liquid holdup for location z/D = 521 as function of for different liquid mass fluxes at 1.4 bar pressure.

the structure frequency does not show any significant axial change. Wolf et al. (2001) have also reported that the frequency of disturbance waves in annular flow (U^*_{GS} > 1.0) does not change beyond z/D = 150.

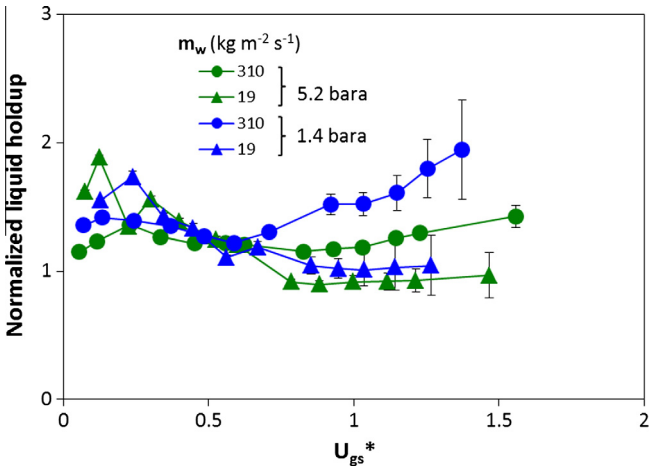

Fig. 13. Normalized liquid holdup for location z/D = 521 as function of for different liquid mass fluxes and pressures.

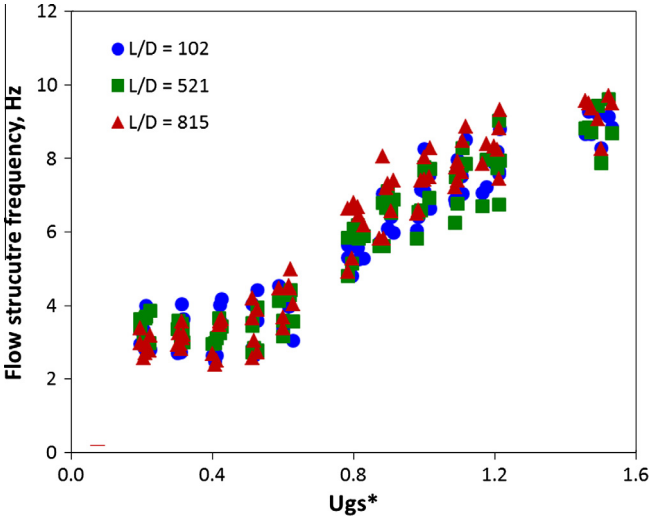

Fig. 14. Flow structure frequency as function of U^*_{GS} for different axial position for the whole range of liquid mass fluxes.

The method developed by Hazuku et al. (2008) for annular flow was also applied to calculate the slug frequency for the tests at U^*_{GS} = 0.05, and the results are presented in Fig. 16. The accuracy of this method was confirmed through visual observation. However, using the visual observations to process all experimental runs would prove extremely time consuming. For U^*_{GS} = 0.05, a significant axial change in slug frequency can be observed, which would be expected due to the coalescence of the Taylor bubbles as a consequence of the axial change in gas velocity. The axial change in gas velocity is in turn caused by elevated pressure gradients that are created at greater values of liquid holdup (see Fig. 10).

The frequencies of annular and churn flow structures and of liquid slugs presented in Figs. 14 and 16 were written in terms of the Strouhal number as a function of the Martinelli parameter as suggested by Kaji et al. (2009), who derived an empirical relationship based on data from several sources for different pipe diameters (ranging from 5 to 150 mm). Since the Strouhal number is a dimensionless parameter used to describe periodic flows, the present authors sought to extend the analysis of Kaji et al. (2009) to annular and churn flow conditions for their periodic flow characteristics. As shown in Fig. 17, the data obtained in the

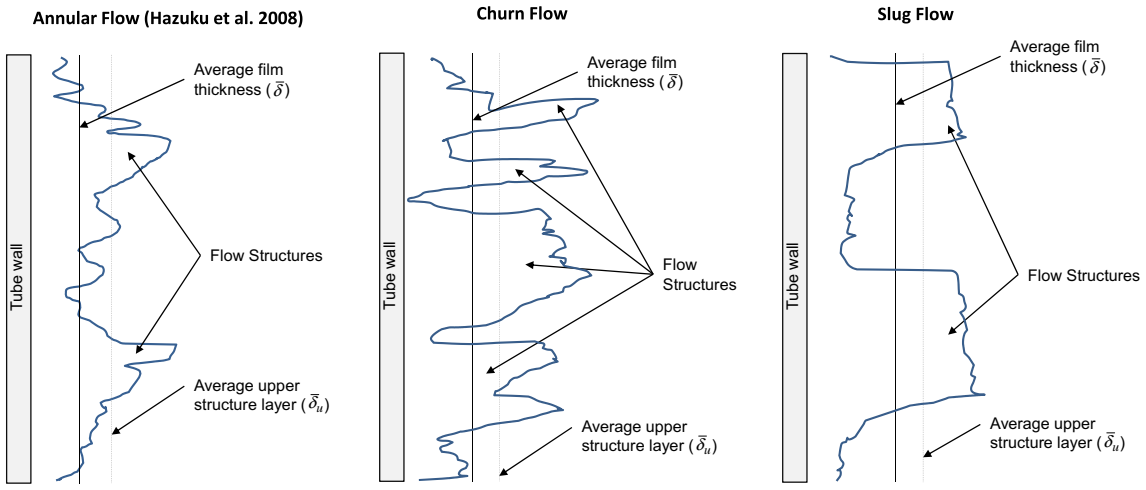

Fig. 15. Qualitative description of the flow structure parameters used in the calculation of the structure frequency.

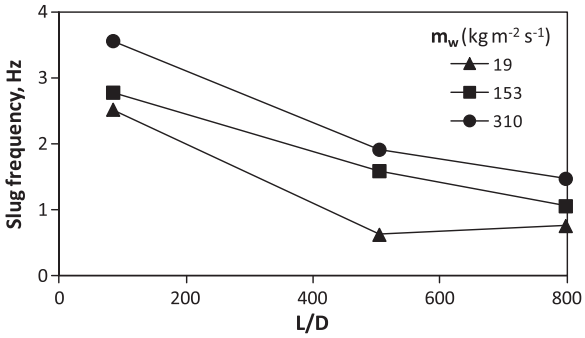

Fig. 16. Slug frequency as function of axial position for $U^*_{GS} = 0.05$, at 1.4 bar pressure.

present work provide a satisfactory extension of the Kaji et al. database. The Strouhal number based on gas superficial velocity is defined as,

$$St_G = \frac{fD}{U_{GS}} \tag{15}$$

where f is the flow structure frequency. In Fig. 17, X is the Martinelli parameter calculated using the superficial liquid and gas velocities ($X = \sqrt{[(dp/dz)_{SL}/(dp/dz)_{SG}]}$).

As mentioned above, the Strouhal number analysis of Kaji et al. (2009) only included slug flow conditions. The experimental data used in the comparison in Fig. 17 include 273 measurements of frequency of large liquid fraction structures in co-current vertical two-phase flows, such as slugs (in slug flow) and waves (in churn or annular flow), for a range of dimensionless superficial gas velocities between 0.05 and 1.5, and pressures between 1.4 and 5.2 bar.

4. Conclusions

The axial development of annular, churn and slug flows in a long vertical flow loop has been investigated. The following conclusions can be drawn from the experimental results:

1. Using video recordings and PDF analyses of liquid holdup for three different axial positions (z/D = 102, 521 and 815), it was possible to observe similarities between the slug flow entrance region of Dukler and Taitel (1986) and churn flow, which has been the source of some confusion previously in the literature, as far as the existence of churn flow as a separate flow regime is concerned. The video recordings and PDF results allowed verification of the occurrence of fully developed churn flow far from the entrance.
2. The occurrence of slug flow at positions far from the liquid inlet (z/D = 480 and 820) is in reasonable agreement with the transition models of Brauner and Barnea (1986) and Jayanti and Hewitt (1992) for low pressures (1.4 bar) and superficial liquid velocities. However, these models do not match the data well for higher pressures (3.8 bar). On the other hand, the transition line of the Hewitt and Roberts (1969) flow map presented a better match at higher rather than lower pressures.
3. The Wallis (1969) criterion and the Turner et al. (1969) critical velocity for the churn-to-annular flow transition were verified against the experimental data. The results showed good agreement between Wallis criterion and the experimental results for

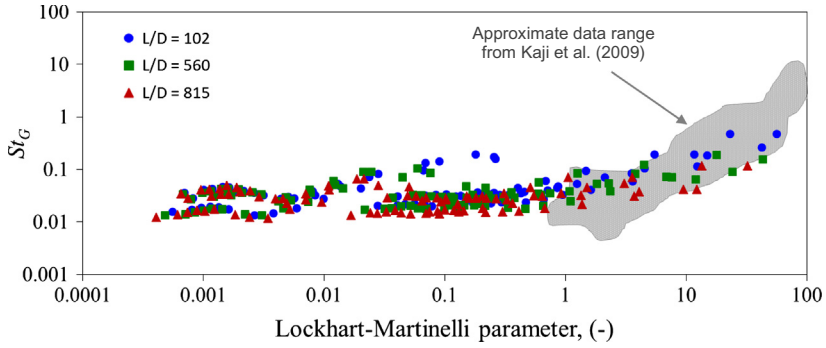

Fig. 17. Annular and churn flow structure and slug frequencies using Strouhal number as a function of the Lockhart–Martinelli parameter. These plot shows a comparison between the approximate database range from Kaji et al. (2009) and the experimental data obtain from the present work.

z/D = 480 and 820 for pressures of 1.4 and 3.8 bar, while the Turner et al. critical velocity only showed good agreement for high superficial liquid velocities.

4. The liquid holdup was seen to vary significantly between all three axial positions (z/D = 102, 521 and 815) for liquid mass flux of 310 kg/m^2-s, while for 19 kg/m^2-s it reached a sort of developed flow for most conditions tested. However, the axial variation of liquid holdup was more pronounced at low pressure levels (1.4 bar).
5. The frequency of flow structures did not present a significant axial variation for U_{GS}^{*} between 0.2 and 1.6. However, for the low gas flow rate conditions at which slug flow was observed, the slug frequency changed considerably in the axial direction. This axial change in the slug frequency is related to axial variation in gas velocity.
6. The experimental data showed that, for different axial locations and flow regimes (slug, churn and annular flow) and a wide range of dimensionless superficial gas velocities, the frequency of the flow structures was well correlated using a Strouhal number based on the superficial gas velocity. The experimental data also showed a reasonable fit with the databank presented by Kaji et al. (2009), which includes a databank from 12 different works previously published in the literature covering pipe diameters ranging from 5 to 150 mm. However, the analysis presented by Kaji et al. only included slug flow conditions, while the present work shows that the Strouhal number can be extended to correlate the flow structures frequency for long vertical tubes (z/D up to 815) and for annular and churn flow conditions.

Acknowledgments

The authors would like to thank the sponsors (Petrobras, RWE and Shell) of the Joint Industry Project on "Liquid Loading in the Operation of Gas Fields: Mechanisms, Prediction and Reservoir Response" at Texas A&M University for supporting this work.

Appendix A. Supplementary material

Supplementary data associated with this article can be found, in the online version, at http://dx.doi.org/10.1016/j.ijmultiphaseflow.2013.06.008.

References

Azzopardi, B.J., Wren, E., 2004. What is entrainment in vertical two-phase churn flow? Int. J. Multiph. Flow 30, 89–103.
Barbosa, J.R., Govan, A.H., Hewitt, G.F., 2001. Visualisation and modelling studies of churn flow in a vertical pipe. Int. J. Multiph. Flow 27, 2105–2127.
Brauner, N., Barnea, D., 1986. Slug/Churn transition in upward gas-liquid flow. Chem. Eng. Sci. 41, 159–163.
Brennen, C.E., 2005. Fundamentals of Multiphase Flow, third ed. Cambridge University Press.
Brown, D.J., Jensen, A., Whalley, P.B., 1975. Non-equilibrium effects in heated and unheated annular two-phase flow. ASME Paper 75, 754–757.
Collier, J.G., Thome, J.R., 1996. Convective Boiling and Condensation, third ed. Oxford University Press, USA.
Costigan, G., 1997. Flow Pattern Transitions in Vertical Gas–Liquid Flows. PhD Thesis, University of Oxford, UK.
Da Riva, E., Del Col, D., 2009. Numerical simulation of churn flow in a vertical pipe. Chem. Eng. Sci. 64, 3753–3765.
Dukler, A.E., Taitel, Y., 1986. Flow Pattern Transition in Gas–Liquid Systems: Measurement and Modeling. Hemisphere Publishing Co., New York.
Ghiaasiaan, S.M., 2007. Two-Phase Flow, Boiling, and Condensation: In Conventional and Miniature Systems. Cambridge University Press.
Hazuku, T., Takamasa, T., Matsumoto, Y., 2008. Experimental study on axial development of liquid film in vertical upward annular two-phase flow. Int. J. Multiph. Flow 34, 111–127.
Hewitt, G.F., 2010, Flooding and flow reversal, In: Thermopedia, Hewitt, G.F., Barbosa, J.R. (Eds.), doi:10.1615/AtoZ.f.flooding_and_flow_reversal.
Hewitt, G.F., Jayanti, S., 1993. To churn or not to churn. Int. J. Multiph. Flow 19, 527–529.
Hewitt, G.F., Martin, C.J., Wilkes, N.S., 1985. Experimental and modelling studies of annular flow in the region between flow reversal and the pressure drop minimum. PhysicoChem. Hydrodyn. 6, 69–86.
Hewitt, G.F., Roberts, D.N., 1969. Study of two-phase flows patterns by simultaneous X-ray and flash photography. Atomic Energy Research Establishment, Berkshire, UK.
Jayanti, S., Hewitt, G.F., 1992. Prediction of the slug-to-churn flow transition in vertical two-phase flow. Int. J. Multiph. Flow 18, 847–860.
Jayanti, S., Hewitt, G.F., Low, D.E.F., Hervieu, E., 1993. Observation of flooding in the Taylor bubble of co-current upwards slug flow. Int. J. Multiph. Flow 19, 531–534.
Julia, J.E., Ozar, B., Dixit, A., Jeong, J.J., Hibiki, T., et al., 2009. Axial development of flow regime in adiabatic upward two-phase flow in a vertical annulus. J. Fluids Eng–T ASME 131, 0213021–02130211.
Lee, J.Y., Kim, N.S., Ishii, M., 2008. Flow regime identification using chaotic characteristics of two-phase flow. Nucl. Eng. Des. 238, 945–957.
Kaji, R., Azzopardi, B.J., Lucas, D., 2009. Investigation of flow development of co-current gas–liquid vertical slug flow. Int. J. Multiph. Flow 35, 335–348.
Mao, Z.S., Dukler, A.E., 1993. The myth of churn flow? Int. J. Multiph. Flow 19, 377–383.
Mi, Y., Ishii, M., Tsoukalas, L.H., 1998. Vertical two-phase flow identification using advanced instrumentation and neural networks. Nucl. Eng. Des. 184, 409–420.
Photron FASTCAM Viewer for High Speed Digital Imaging, 2006, 3.28.2 ed. Photron, California.
Pushkina, O.L., Sorokin, Y.L., 1969. Breakdown of liquid film motion in vertical tubes. Heat Transfer Sov. Res. 1, 56–64.
Turner, R.G., Hubbard, M.G., Dukler, A.E., 1969. Analysis and prediction of minimum flow rate for the continuous removal of liquids from gas wells. SPE J. Petrol. Technol. 21, 1475–1482.
Van Hout, R., Barnea, D., Shemer, L., 2001. Evolution of statistical parameters of gas–liquid slug flow along vertical pipes. Int. J. Multiph. Flow 27, 1579–1602.
Wallis, G.B., 1969. One-Dimensional Two-Phase Flow. McGraw-Hill, New York.
Wang, K., Bai, B., Cui, J., Ma, W., 2012. A physical model for huge wave movement in gas–liquid churn flow. Chem. Eng. Sci. 79, 19–28.
Wolf, A., Jayanti, S., Hewitt, G.F., 2001. Flow development in vertical annular flow. Chem. Eng. Sci. 56, 3221–3235.
Zabaras, G., Dukler, A.E., Moalem-Maron, D., 1986. Vertical upward cocurrent gas–liquid annular flow. AIChE J. 32, 829–843.